Optics & Laser Technology 154 (2022) 108294

Contents lists available at ScienceDirect

Optics and Laser Technology

journal homepage: www.elsevier.com/locate/optlastec

Sector-based Fresnel zone plate with extended depth of focus

Francisco Jose Torcal-Milla [a,b,*], Luis Miguel Sanchez-Brea [b], Jose Antonio Gomez-Pedrero [c]

[a] Applied Physics Department, Grupo de Tecnología Óptica Láser, Instituto de Investigacion en Ingenieria de Aragon (i3a), University of Zaragoza, C/ Pedro Cerbuna 12, 50009 Zaragoza, Spain
[b] Applied Optics Complutense Group, Optics Department, Faculty of Physics, Universidad Complutense de Madrid, Plaza de las Ciencias 1, 28040 Madrid, Spain
[c] Applied Optics Complutense Group, Optics Department, Faculty of Optics and Optometry, Universidad Complutense de Madrid, C/ Arcos de Jalón 118, 28037 Madrid, Spain

ARTICLE INFO

Keywords:
Diffractive lens
Fresnel zone plate
Extended depth of focus
Diffraction

ABSTRACT

A Sector-based Fresnel zone plate consists of a binary diffractive lens composed of a mosaic of sectors of Fresnel zone plates with different focal distances. When these focal distances are linearly distributed within the sectors, dual focus is obtained. Besides, we explore the possibility to generate an extended depth-of-focus lens by using a cubic distribution of the focal distances assigned to the sectors and optimizing the weight factors given to the terms of the cubic polynomial. Finally, numerical simulations based on the Rayleigh-Sommerfeld approach are carried out and experimental verifications by using a Spatial Light Modulator are performed, showing high agreement. The proposed kind of zone plate has potential applications in different research fields such as microscopy, lithography, data storage, or imaging.

1. Introduction

Extended depth of focus (EDOF) lenses are used in a large number of techniques such as optical coherence tomography, microscopy, imaging, data storage, or micro-lithography [1–10]. Among other possibilities, EDOF lenses can be generated by combining a conventional lens with a diffractive optical element (DOE), which modulates the amplitude or/and the phase of the incident beam. Mixed DOEs have better axial homogeneity but suffer of low efficiency. Consequently, phase-based and amplitude-based DOEs have reached more popularity since more impinging energy is transmitted with phase-based DOEs [11–13], and binary amplitude-based DOEs are easier to be manufactured, respectively. EDOF lenses have been analyzed from different points of view [14]. Some authors combine refractive and diffractive elements by using Spatial Light Modulators (SLM) or other active elements [15–18]. Flores et al. show how an achromatic hybrid element can be optimized to obtain a deeper focal distance, ten times better than the conventional equivalent refractive lens [19]. Zhao et al. show how the usage of an optimized sinusoidal phase mask improves the depth of field of a conventional lens by coding the wavefront [20]. Other authors use pure phase diffractive optical elements [21], or angularly dependent optical elements [22–25], to extend the depth of focus.

Regarding the design of the optical elements and their optimization, computational methods may improve the optical performance of the optical systems. In this way, Elmalem et al. propose a complex computational image-based technique based on the synergy between a simple phase aperture coding optical element and a convolutional neural network [26]. Besides, more complex algorithms which involve not only calculating the EDOF optical element, but also optimizing its characteristics to produce a given intensity distribution along the optical axis have been proposed and analyzed [27–30].

In this work, we propose a new kind of diffractive lens composed by a mosaic of sectors of Fresnel zone plates (FZP) with different focal lengths. When the number of sectors is low, the focus is quite noisy, but this is solved by using a high number of sectors. From the numerical analysis, we obtain the dependency of the depth of focus and the focal width on the design parameters of the zone plate. When the focal distances assigned to the sectors are linearly distributed, the diffractive optical element produces dual-focus. Then, we analyze a cubic distribution of the focal distances, showing that EDOF is obtained. The Sector-based Fresnel zone plates are numerically implemented by using the Rayleigh-Sommerfeld approach and finally, we corroborate their performance with experiments by using a Spatial Light Modulator (SLM), showing high agreement between simulations and experiments.

* Corresponding author.
E-mail address: fjtorcal@unizar.es (F.J. Torcal-Milla).

https://doi.org/10.1016/j.optlastec.2022.108294
Received 3 September 2021; Received in revised form 4 April 2022; Accepted 12 May 2022
Available online 24 May 2022

2. Sector-based Fresnel zone plate with equi-distributed focal distances

As it is well known, a Fresnel zone plate is a binary diffractive lens formed by alternating transparent and opaque rings whose radii are approximately given by $r_m = \sqrt{m\lambda f}$, where m is the ring order, λ the design wavelength and f the focal length [31]. An example of amplitude-based FZP is shown in Fig. 1a. As we will show along the manuscript, we have considered amplitude-based binary DOEs for our analysis since they are easier to be manufactured. Nevertheless, all conclusions are still valid for binary phase-based DOEs with the same spatial distribution. When a conventional FZP is illuminated with a collimated Gaussian beam in normal incidence, the main parameters of the focus are the focal width, ω_0, and the depth of focus (DOF) [32],

$$\omega_0 = \frac{2\lambda}{\pi}\frac{f}{D}, \qquad (1)$$

$$DOF = \frac{2\pi\omega_0^2}{\lambda} = \frac{8\lambda}{\pi}\left(\frac{f}{D}\right)^2,$$

where D is the diameter of the lens.

DOF can be increased by reducing the lens diameter or increasing the focal length. However, the focal width is also increased. An alternative to increase the DOF is the use of angular diffractive lenses, such as Daisy or Lotus lenses [25]. The Daisy lens produces always dual focus but Lotus lenses can be optimized to reduce the beam width at the center of the dual focus [33], since the histogram of the focal distances produced by the Lotus lens is equi-distributed.

Another possibility, which is explored in this work, is to increase the DOF by using a Sector-based Fresnel zone plate (SFZP). It consists of a diffractive lens composed of a mosaic of circular sectors of FZP with different focal distances. The simplest configuration is to divide the area of the lens in n_f angular sectors, with equal size. The focal distances for each sector are $f_{1,j} \in \{f_{1,1}, f_{1,2}, \ldots, f_{1,n_f}\}$ and they can be regularly distributed within the interval $[\bar{f} - \Delta f/2,\ \bar{f} + \Delta f/2]$, Fig. 1b. Then, the focal length associated to the sector i is

$$f_{1,i} = \left(\bar{f} - \Delta f \Big/ 2\right) + \Delta f \frac{i}{n_f}, \qquad (2)$$

where $i = 1, 2, \ldots, n_f$. When the number of sectors is low, the intensity distribution around the focus is quite random and with a number of artifacts, Fig. 2b, in comparison with a Fig. 2a. This intensity distribution has been obtained by a numerical implementation of the Rayleigh-Sommerfeld formula [34,35].

To deal with this issue, one possibility is to increase the number of slices. For this, we have subdivided each sub-sector in n_s equi-spaced randomly distributed zones. Then, the number of slices is $n_f \times n_s$. An example, for $n_f = 10$ and $n_s = 10$, is shown in Fig. 1c. In this case, when the SFZP is formed by a high number of sectors with equal size and linearly distributed focal distances, dual focus is obtained,Fig. 2c.

To check the performance of the lenses, we have also obtained the XY intensity distribution at the central focal distance, $z = \bar{f}$, Fig. 3. We see that the central intensity distribution is circular but, for the case of $n_f = 10, n_s = 10$, a halo around the focus is produced, Fig. 3c. To eliminate it, we have increased the number of sectors to $n_f = 50, n_s = 50$ and then, the focus becomes more uniform without spurious light around it, Fig. 3d. Dual focus can be observed when the number od sectors is $n_s =$

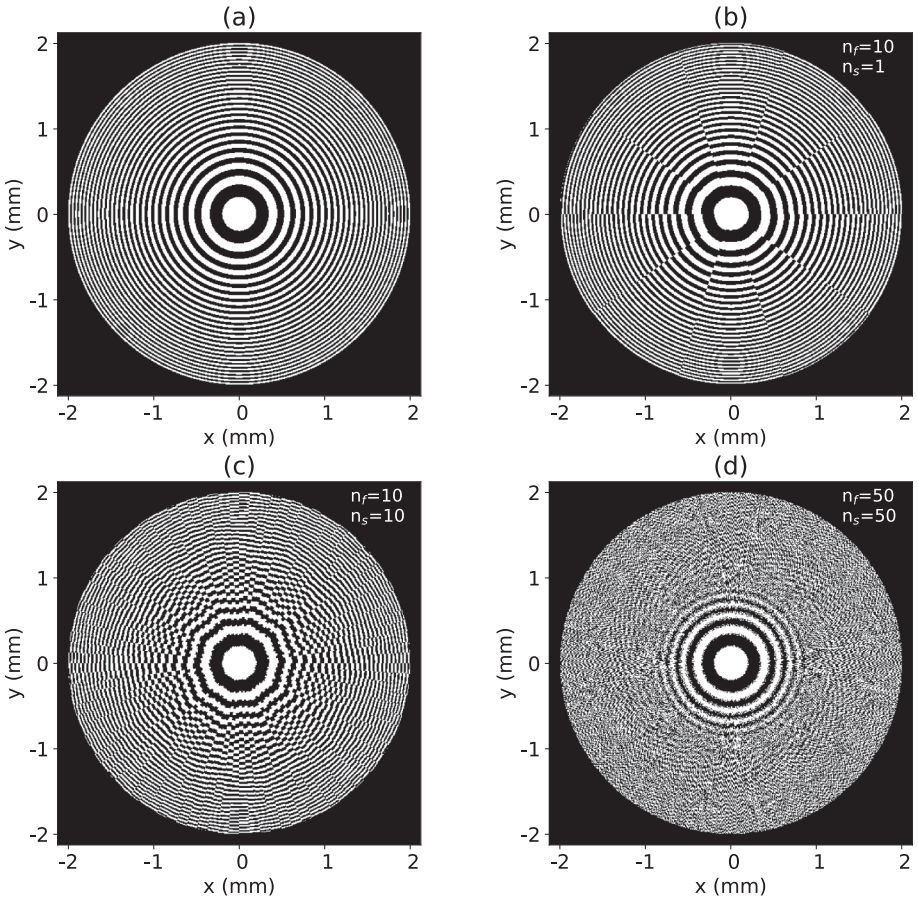

Fig. 1. (a) Conventional amplitude-based Fresnel zone plate with $\bar{f} = 125$ mm. (b) - (d) are SFZP with $\bar{f} = 125$ mm and $\Delta f = 12.5$ mm. The n_s and n_f parameters are defined in each subfigure. For all the cases, the design wavelength is $\lambda = 632.8$ nm.

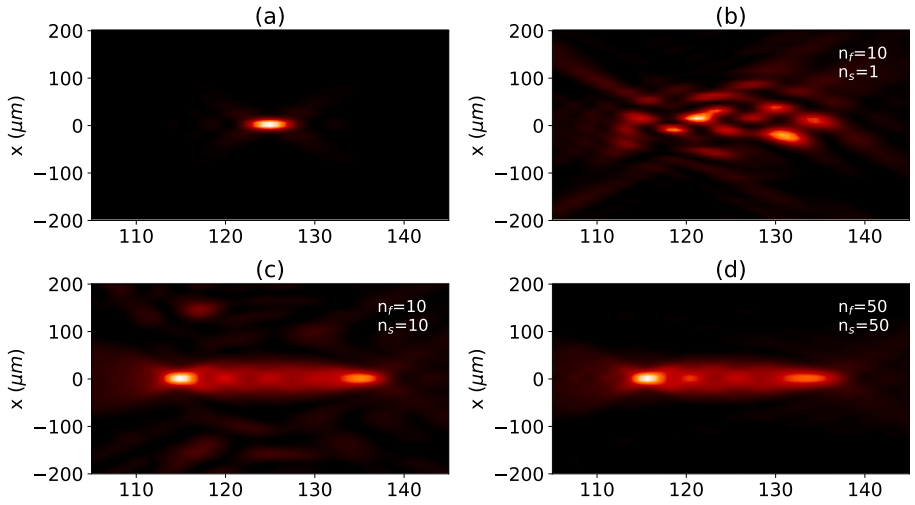

Fig. 2. Intensity distribution XZ, obtained by numerical Rayleigh-Sommerfeld formula, for the lenses depicted in Fig. 1. The illumination is a plane wave with wavelength $\lambda = 632.8\ nm$.

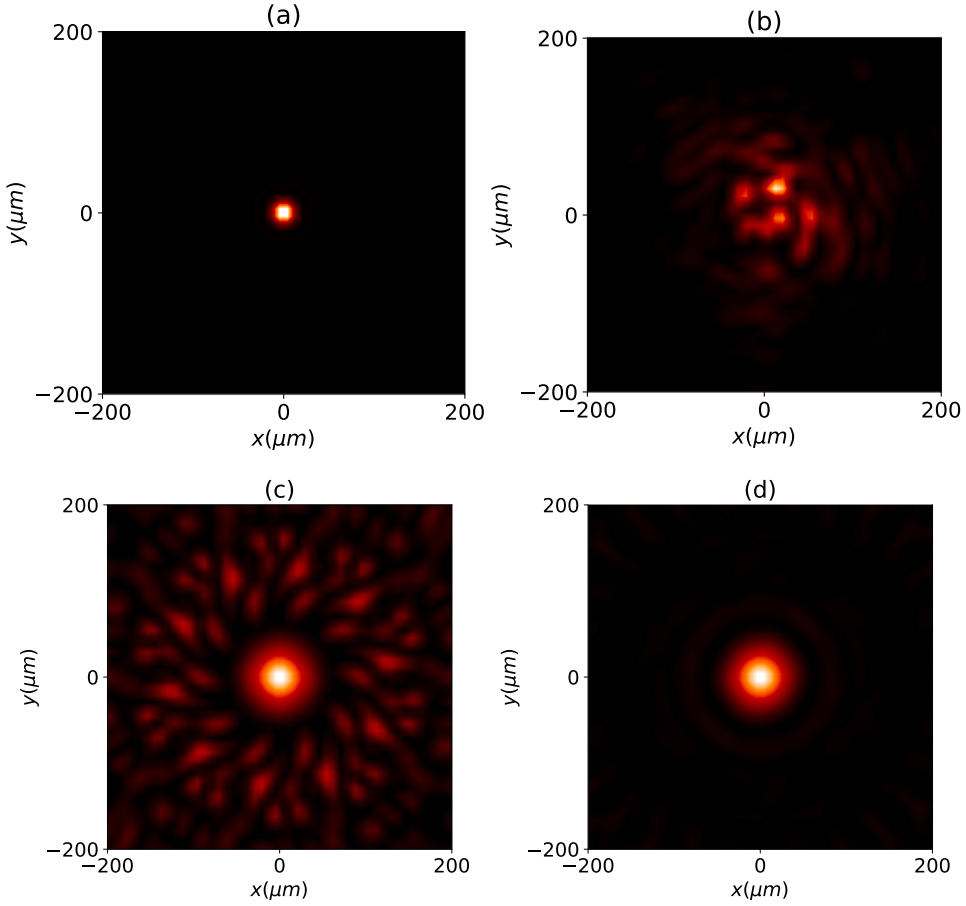

Fig. 3. Intensity distribution XY, obtained by numerical Rayleigh-Sommerfeld formula, for the lenses depicted in Fig. 1. The illumination is a plane wave with wavelength $\lambda = 632.8\ nm$ and the observation distance is $z = \bar{f}$. The beam width in Figs. 3c and 3d is greater since the narrow intensity distribution is obtained at $z = \bar{f} \pm \Delta f/2$, not at $z = \bar{f}$.

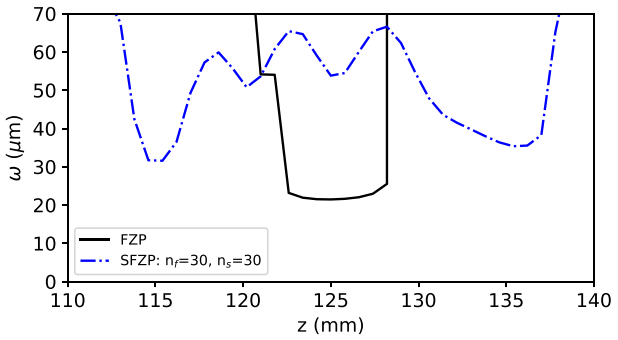

Fig. 4. Beam width, measured by FWHM parameter, for the FZP and the SFZP described in Fig. 2a and Fig. 2d.

10 (Fig. 2c) or $n_s = 50$ (Fig. 2d).

Finally, the beam width, measured as the Full Width at Half Maximum (FWHM) of the XYZ intensity distribution around the focus, for the FZP and the SFZP with $n_f = 50, n_s = 50$, is shown in Fig. 4. Dual focus is clear and the two foci are placed at approximately $z = \bar{f} \pm \Delta f/2$. Also, we can see that the two foci are not exactly equal, but they present different beam width and different DOF.

3. Improvement of the Sector-based Fresnel zone plate to achieve EDOF

Now, we will explore the possibility to obtain an extended depth of focus instead of dual-focus with a SFZP. For this, we propose to modify the distribution of focal distances assigned to the sectors. Two problems need to be solved. In the first place, we need to balance the intensity distribution between the two foci produced by the SFZP. This can be solved by modifying the focal distances of the sectors given in Eq. (2), by adding a quadratic term,

$$f_{2,i} = \left(\bar{f} - \Delta f \Big/ 2\right) + \Delta f \left(\frac{i}{n_f}\right)^2. \tag{3}$$

Then, the weighted focal distance for each sector can be obtained as

$$f_i = (1 - k_1) f_{1,i} + k_1 f_{2,i}, \tag{4}$$

where the k_1 parameter can be obtained by a simple optimization. With this quadratic term, the slopes at the edges are different and the most distant focus is more intense.

Also, we need to provide more intensity at zones near the central focus $\bar{f}$. For this, a cubic term is added to the foci distribution

$$f_{3,i} = \bar{f} + 4\Delta f \left(\frac{i - n_f/2}{n_f}\right)^3, \tag{5}$$

and the resulting focal distance assigned to the i-th sector results in

$$f_i = (1 - k_1 - k_2) f_{1,i} + k_1 f_{2,i} + k_2 f_{3,i}, \tag{6}$$

where the k_2 parameter can be also obtained by a simple optimization. With this cubic term, the slope of the central area is reduced, and the weight of the central foci becomes greater. We name the SFZP with quadratic and cubic term as Cubic Sector-based Fresnel Zone Plate (CSFZP). The terms $f_{1,i}$, $f_{2,i}$ and $f_{3,i}$ are shown in Fig. 5a, and an example of how these two terms modify the focal distribution is shown in Fig. 5b.

The effect of these terms on the intensity distribution around the central focus is shown in Fig. 6. The weight parameters have been

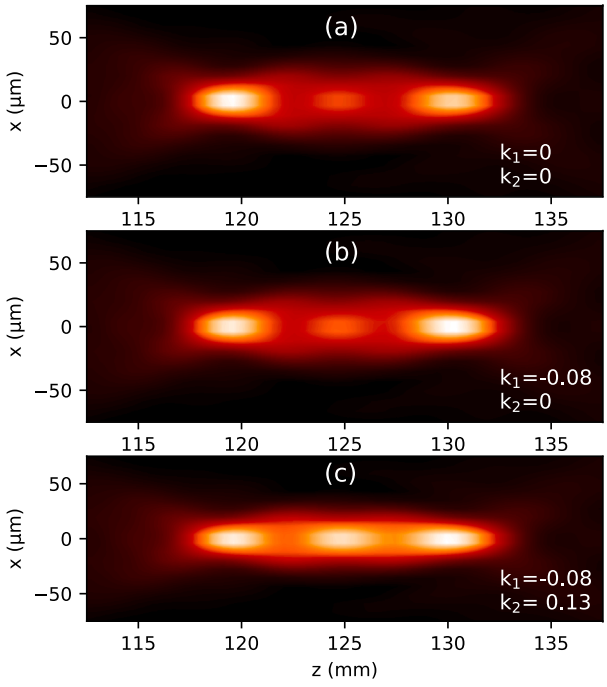

Fig. 6. Intensity distribution XZ around the focus for a lens with $\bar{f} = 125$ mm, $\Delta f = 12.5$ mm, $n_f = 50$, and $n_s = 50$, for different k_1 and k_2 parameters.

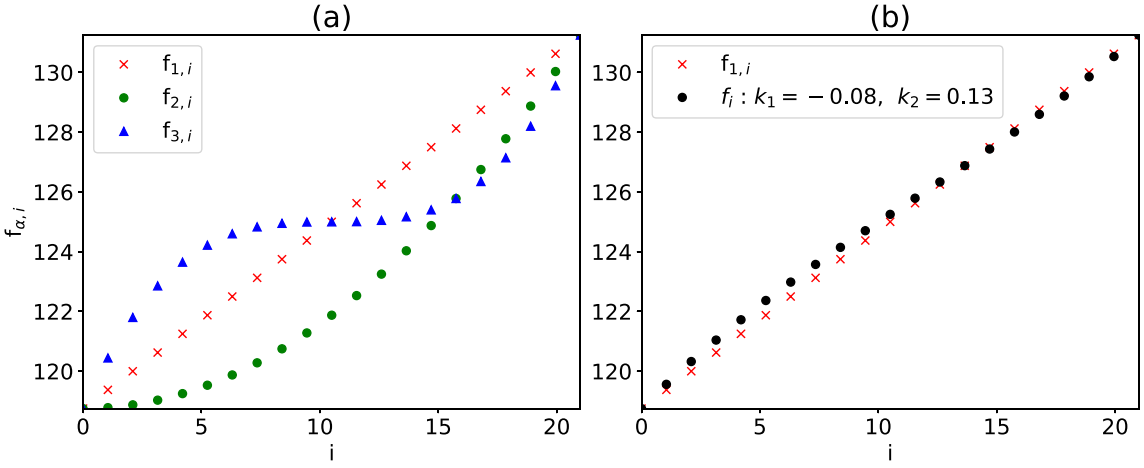

Fig. 5. a) $f_{1,i}, f_{2,i}$, and $f_{3,i}$ focal distances for the linear, quadratic and cubic terms of a lens with $\bar{f} = 125$ mm, $\Delta f = 12.5$ mm, $n_f = 50$, and $n_s = 50$. b) Example of linear combination, Eq. (6) to improve the SFZP behavior.

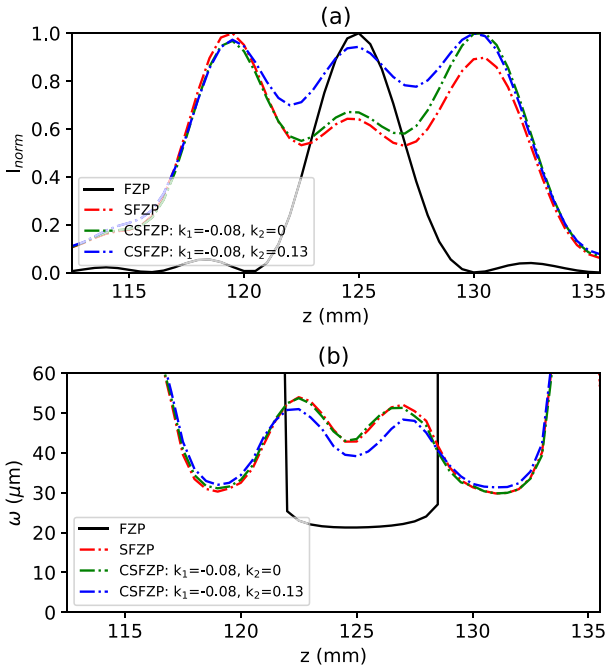

Fig. 7. a) Normalized intensity and b) beam width measured using FWHM parameter for the simulations of Fig. 6.

obtained by optimization. In Fig. 6a, a linear distribution of focal distances, SFZP, is used. Dual focus is obtained, and no balance between the two focus is obtained. In Fig. 6b a quadratic term is added and, as a consequence, the two foci present approximately the same intensity. When a cubic term is added, Fig. 6c, the intensity at the center is also increased to approximately the same level that those of dual focus situation. Here, the intensity distribution seems to be tri-focus, although this fact has not been corroborated experimentally.

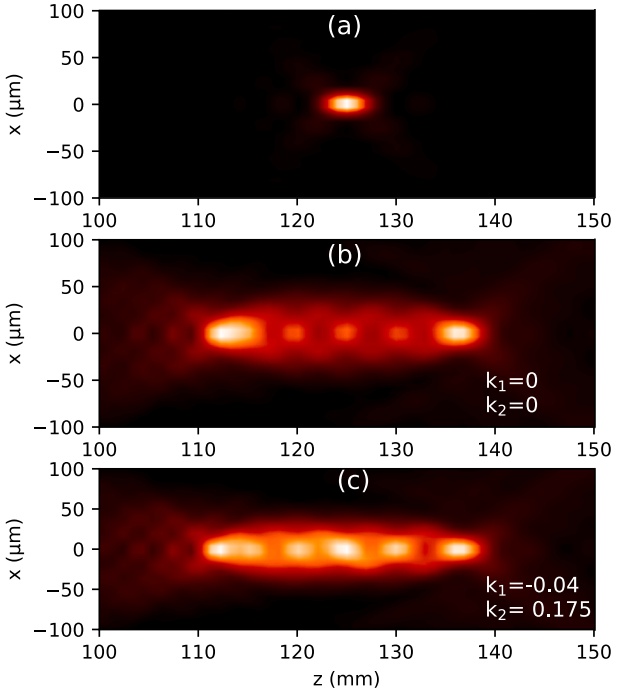

Fig. 8. Intensity distribution XZ around the focus, $\bar{f} = 125$ mm, for a) a FZP lens, b) a SFZP, and c) a CSFZP with $\bar{f} = 125$ mm, $\Delta f = 25$ mm, $n_s = 50$ and $n_f = 50$.

Two interesting parameters to check the behavior of the CSFZP are the intensity at the optical axis and the Full Width at Half Maximum (FWHM). These two parameters are shown in Fig. 7. We see that, although the FWHM has not decreased to the same level that for the dual focus, the intensity at the axis is almost equal.

Finally, we have analyzed the CSFZP behaviour for higher values of the $\Delta f/\bar{f}$ parameter. For example, in Fig. 8 we can see the XZ intensity distribution for a FZP, a SFZP, and a CSFZP. The parameters are the same than those of Fig. 6, with $\bar{f} = 125$, except the Δf parameter, which is $\Delta f = 25$ mm, so that $\Delta f/\bar{f}$=20%. New parameters for the optimization of the CSFZP have been found: $k_1 = -0.04$ and $k_2 = 0.175$. In any case, we can see that the increase in the DOF is notorious and the beam width only increases from FWHM $= 20\ \mu m$ to FWHM $= 35\ \mu m$.

4. Experimental approach

An experimental verification of the focusing behavior of the CSFZP has been performed by using a SLM. The scheme of the set-up is shown in Fig. 9. The light source is a polarized He-Ne laser ($\lambda = 632.8$ nm). A spatial filter, formed by a 40x microscope objective (OBJ), a 10μm pinhole (PH), and a collimating lens (CL), is used to expand the beam so that the SLM is completely illuminated. A quarter wave plate (QW) is used to obtain circular polarization, and two linear polarizers (P) and two additional quarter wave plates (QW) are used to obtain the desired levels of intensity [36]. The SLM is a Holoeye LCR-2500 reflective light modulator. It has 1024 × 768 pixels (8 bits resolution) whose pixel size is 19μm × 19μm. A 50/50 beam-splitter (BS) is placed at 45° with the propagation axis, thus the SLM is illuminated normally to its surface. An image-relaying system, formed by two lenses with foci $f_1 = 80\,mm$ and $f_2 = 60\,mm$, is used to produce an image of the Sector-based Fresnel zone plates at a plane near to the linear stage and, also to reduce its size in a factor $f_2/f_1 = 0.75\times$. A 72BUC02-ML CMOS camera (Imaging source) is placed on a SMC100 linear stage (Newport). The CMOS camera has 2592 × 1944 pixels with a pixel size of 2.2μm × 2.2μm. The camera is free to travel along the beam propagation axis, so we can measure the intensity distribution at any desired plane after the lens. The aberrations of the wavefront have been removed by adding a phase map to the zone plates implemented within the SLM [25].

To validate the numerical results and check that the CSFZP is a valid lens to obtain EDOF, the XYZ intensity distribution around the focus has been measured and analyzed for a FZP, a SFZP and a CSFZP. The focal

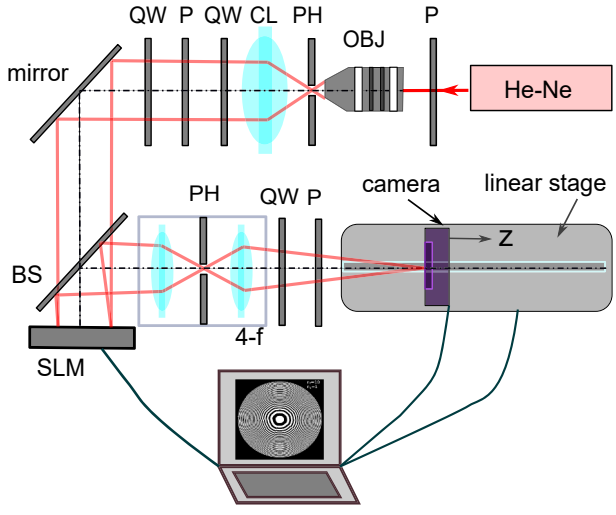

Fig. 9. Experimental setup. He-Ne: He-Ne laser, OBJ: microscope objective, PH: pinhole, CL: collimation lens, P: linear polarizer, QW: quarter waveplate, BS: 50/50 beam-splitter, and SLM: Spatial Light Modulator. The camera is placed on a linear stage and it is free to travel along the beam propagation axis.

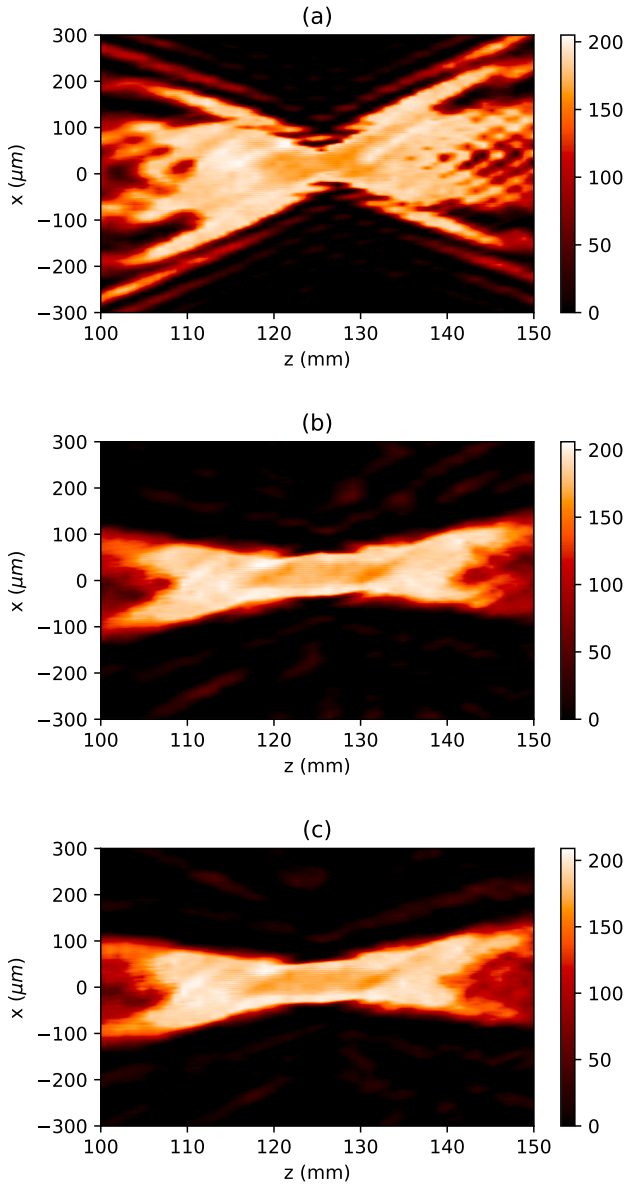

Fig. 10. Experimental intensity distribution at focus for (a) FZP (b) SFZP, and (c) CSFZP. The focal distance for this lenses is $\bar{f} = 125mm$ and the diameter is $D = 4mm$. For the SFZP and the CSFZP, $\Delta f = 12.5mm$.

length of the lenses is $\bar{f} = 125mm$ and the diameter of the lenses is $D = 4mm$. For the SFZP and the CSFZP, $\Delta f = 12.5mm$ ($\Delta f/f = 10\%$). In Fig. 10 we show the experimental XZ intensity profiles for these lenses. The SFZP and the CSFZP are quite similar but there is not an increase of the beam width at $z = \bar{f}$ for the CSFZP. This effect, predicted numerically, is more clear in Fig. 12a, where the FWHM for the FZP, SFZP and CSFZP is obtained. It is clear that SFZP and CSFZP present a longer DOF. Also, we can see that the CSFZP is not dual focus, but it presents a continuous beam width. Nevertheless, the parameters predicted in Eq. (6) does not seem to be the accurate for the experiment.

We have also implemented a CSFZP with a longer $\Delta f = 25mm$ ($\Delta f/f = 20\%$), Fig. 11. In this case, the foci of the SFZP and the CSFZP are clearly longer than for the FZP. As predicted in the previous section, the SFZP is dual focus and EDOF is obtained for the CSFZP.

Fig. 12 shows the experimental FWHM parameter for the three lenses. The characteristic parameters obtained using these experimental data are shown in Table 1. The DOF, is approximately $3.5mm$ for the FZP, and $24mm$ for the CSFZP. On the other hand, the beam width

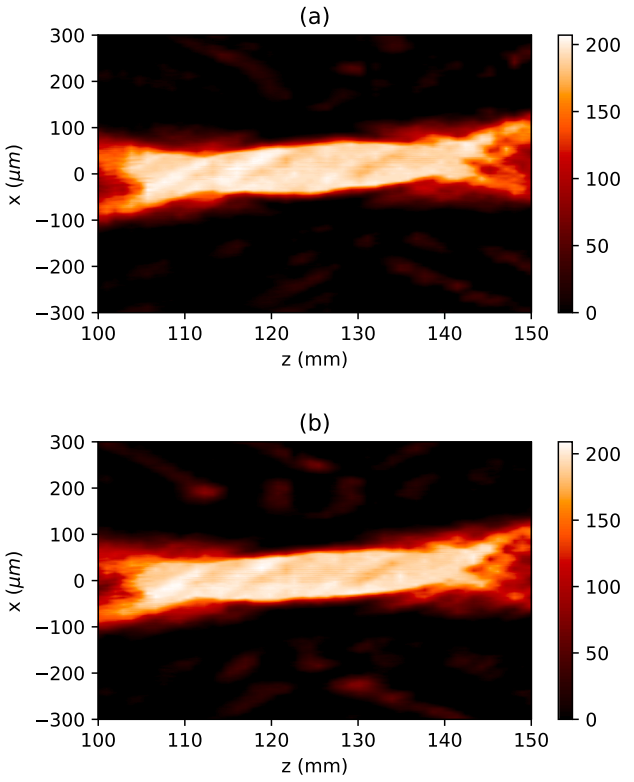

Fig. 11. Experimental intensity distribution around focus for a) SFZP, and b) CSFZP. The focal distance for this lenses is $\bar{f} = 125mm, \Delta f = 25mm$, and the diameter is $D = 4mm$.

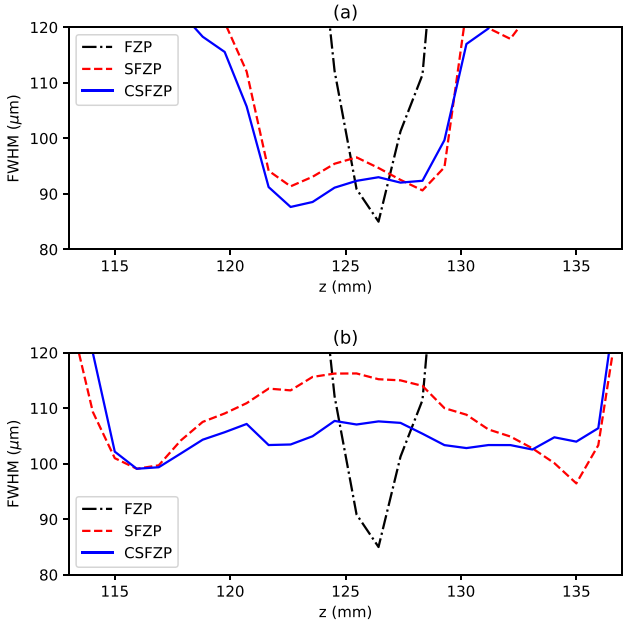

Fig. 12. Comparison of the experimental FWHM for FZP, SFZP and CSFZP, computed from XYZ profiles (a) for the experiment of Fig. 10 and (b) for the experiment of Fig. 11.

increases from $85\mu m$ for the FZP to $106\mu m$ for the CSFZP. Then, DOF is increased approximately 7 times while beam width is increased only 1.25 times.

Table 1
Focus parameters obtained with the experiment shown in Fig. 11.

Lens	DOF (mm)	FWHM (μm)
FZP	3.5	85
SFZP	25	115
CSFZP	24	106

5. Conclusions

In this work, we propose and analyze a new kind of diffractive lens named Sector-based Fresnel zone plate. It is formed by a mosaic of circular sectors of Fresnel zone plates with different focal distances. As we demonstrate, this zone plate can be used to generate dual or extended depth-of focus, depending on the distribution of focal distances assigned to the sectors. We show that, when the focal distances assigned to the sectors are equi-distributed, dual focus is obtained. On the other hand, when a cubic distribution of the foci assigned to the sectors is used, Extended Depth of Focus is obtained. Numerical simulations, based on the Rayleigh-Sommerfeld approach, have been carried out and experimental verifications have been performed by using a Spatial Light Modulator. The numerical and experimental results show high agreement, which makes the proposed zone plate to be an insteresting alternative in applications related to microscopy, lithography, data storage, or imaging.

Declaration of Competing Interest

The authors declare that they have no known competing financial interests or personal relationships that could have appeared to influence the work reported in this paper.

Acknowledgments

This work has been funded by project Retos Colaboración 2019 “Teluro” RTC2019-007113–3 of the Ministerio de Economía y Competitividad and the European Union, European funds for regional development and by project Gobierno de Aragón-Fondo Social Europeo (Grupo de Tecnología Óptica Láser— E44_20R), and European Fund for Regional Development (EFRD-FEDER, EU) and the Spanish Government’s Agencia Estatal de Investigación (AEI) through the grant DPI2016-75272-R.

References

[1] Z. Liu, A. Flores, M.R. Wang, J.J. Yang, Diffractive infrared lens with extended depth of focus, Opt. Eng. 46 (1) (2007) 018002.
[2] C. Perwass, L. Wietzke, “Single lens 3D-camera with extended depth-of-field,” in Human Vision and Electronic Imaging XVII, vol. 8291. International Society for Optics and Photonics, 2012, p. 829108.
[3] T. Kohnen, M. Böhm, E. Hemkeppler, S. Schönbrunn, N. DeLorenzo, K. Petermann, M. Herzog, Visual performance of an extended depth of focus intraocular lens for treatment selection, Eye 33 (10) (2019) 1556–1563.
[4] S.C. Schallhorn, D. Teenan, J.A. Venter, S.J. Hannan, J.M. Schallhorn, Initial clinical outcomes of a new extended depth of focus intraocular lens, J. Refract. Surg. 35 (7) (2019) 426–433.
[5] C. Shen, Q. Hong, Q. Zhu, C. Zu, S. Wei, Holographic projection based on programmable axilens, Opt. Laser Technol. 120 (2019) 105682.
[6] R. Rampat and D. Gatinel, “Multifocal and extended depth-of-focus intraocular lenses in 2020,” Ophthalmology, 2020.
[7] D. Lorenser, X. Yang, D.D. Sampson, Ultrathin fiber probes with extended depth of focus for optical coherence tomography, Opt. Lett. 37 (10) (2012) 1616–1618.
[8] R. Leitgeb, M. Villiger, A. Bachmann, L. Steinmann, T. Lasser, Extended focus depth for Fourier domain optical coherence microscopy, Opt. Lett. 31 (16) (2006) 2450–2452.
[9] B. Yin, C. Hyun, J.A. Gardecki, G.J. Tearney, Extended depth of focus for coherence-based cellular imaging, Optica 4 (8) (2017) 959–965.
[10] V. Pal, C. Tradonsky, R. Chriki, N. Kaplan, A. Brodsky, M. Attia, N. Davidson, A. A. Friesem, Generating flat-top beams with extended depth of focus, Appl. Opt. 57 (16) (2018) 4583–4589.
[11] R. Liu, B.-Z. Dong, G.-Z. Yang, B.-Y. Gu, Generation of pseudo-nondiffracting beams with use of diffractive phase elements designed by the conjugate-gradient method, J. Opt. Soc. Am. A 15 (1) (1998) 144–151.
[12] S. Ledesma, J. Escalera, J. Campos, J. Mazzaferri, M.J. Yzuel, High depth of focus by combining annular lenses, Opt. Commun. 266 (1) (2006) 6–12.
[13] D. Zalvidea, C. Colautti, E.E. Sicre, Quality parameters analysis of optical imaging systems with enhanced focal depth using the wigner distribution function, J. Opt. Soc. Am. A 17 (5) (2000) 867–873.
[14] Z. Zalevsky, Extended depth of focus imaging: a review, SPIE Rev. 1 (1) (2010) 018001.
[15] B. Qi, A.P. Himmer, L.M. Gordon, X.V. Yang, L.D. Dickensheets, I.A. Vitkin, Dynamic focus control in high-speed optical coherence tomography based on a microelectromechanical mirror, Opt. Commun. 232 (1–6) (2004) 123–128.
[16] K. Sasaki, K. Kurokawa, S. Makita, Y. Yasuno, Extended depth of focus adaptive optics spectral domain optical coherence tomography, Biomed. Opt. Exp. 3 (10) (2012) 2353–2370.
[17] P. Gao, S. Tian, X. Weng, H. Guo, Dynamically shifting the focal spot with tunable pupil filters, J. Mod. Opt. 63 (16) (2016) 1558–1563.
[18] S.N. Khonina, A.V. Ustinov, A.P. Porfirev, Dynamic focal shift and extending depth of focus based on the masking of the illuminating beam and using an adjustable axicon, JOSA A 36 (6) (2019) 1039–1047.
[19] A. Flores, M.R. Wang, J.J. Yang, Achromatic hybrid refractive-diffractive lens with extended depth of focus, Appl. Opt. 43 (30) (2004) 5618–5630.
[20] H. Zhao, Y. Li, Optimized sinusoidal phase mask to extend the depth of field of an incoherent imaging system, Opt. Lett. 35 (2) (2010) 267–269.
[21] N. Xu, Z. Kong, Q. Tan, Y. Fu, Multiring pure-phase binary optical elements to extend depth of focus, Appl. Opt. 57 (32) (2018) 9643–9648.
[22] G. Mikula, Z. Jaroszewicz, A. Kolodziejczyk, K. Petelczyc, M. Sypek, Imaging with extended focal depth by means of lenses with radial and angular modulation, Opt. Exp. 15 (15) (2007) 9184–9193.
[23] J.A. Rodrigo, T. Alieva, Freestyle 3d laser traps: tools for studying light-driven particle dynamics and beyond, Optica 2 (9) (2015) 812–815.
[24] V.A. Soifer, S.I. Kharitonov, S.N. Khonina, Y.S. Strelkov, A.P. Porfirev, ”Spiral caustics of vortex beams,” in Photonics, Multidisciplinary Digital Publishing Institute 8 (1) (2021) 24.
[25] L.M. Sanchez-Brea, F.J. Torcal-Milla, J. del Hoyo, A. Cuadrado, J.A. Gomez-Pedrero, Optimization of angular diffractive lenses with extended depth of focus, J. Opt. 22 (2020) 065601.
[26] S. Elmalem, R. Giryes, E. Marom, ”Learned phase coded aperture for the benefit of depth of field extension,” Opt. Exp., vol. 26, no. 12, pp. 15 316–15 331, 2018.
[27] S. Khonina, V. Kotlyar, V. Soifer, Calculation of the focusators into a longitudinal line-segment and study of a focal area, J. Mod. Opt. 40 (5) (1993) 761–769.
[28] L. Doskolovich, N. Kazanskiy, V. Soifer, A.Y. Tzaregorodtzev, Analysis of quasiperiodic and geometric optical solutions of the problem of focusing into an axial segment, Optik-International Journal for Light and Electron Optics 101 (2) (1995) 37–41.
[29] M. Martinez-Corral, M. Caballero, E.H. Stelzer, J. Swoger, Tailoring the axial shape of the point spread function using the toraldo concept, Opt. Exp. 10 (1) (2002) 98–103.
[30] D. Kachalov, V. Pavelyev, S. Khonina, R. Skidanov, O.Y. Moiseev, Application of the direct search in solving a problem of forming longitudinal distribution of intensity, J. Mod. Opt. 58 (1) (2011) 69–76.
[31] O.K. Ersoy, Diffraction, Fourier optics and imaging. John Wiley & Sons, 2006, vol. 30.
[32] B.E.A. Saleh, M.C. Teich, Fundamentals of Photonics, John Wiley & Sons, 2019.
[33] K. Uno, I. Shimizu, Dual focus diffractive optical element with extended depth of focus, Opt. Rev. 21 (5) (2014) 668–675.
[34] L.M. Sanchez-Brea. (2019) Diffractio, Python module for diffraction and interference optics. [Online]. Available: https://pypi.org/project/diffractio/.
[35] F. Shen, A. Wang, Fast-Fourier-transform based numerical integration method for the Rayleigh-Sommerfeld diffraction formula, Appl. Opt. 45 (6) (2006) 1102–1110.
[36] I. Moreno, P. Velásquez, C.R. Fernández-Pousa, M.M. Sánchez-López, F. Mateos, Jones matrix method for predicting and optimizing the optical modulation properties of a liquid-crystal display, J. Appl. Phys. 94 (6) (2003) 3697–3702.